J Therm Anal Calorim (2010) 100:509–517
DOI 10.1007/s10973-009-0654-7

Thermoanalytical and structural characterization of fluoridated calcium phosphates prepared in anhydrous alcohols

Ricardo G. Simões · Ana I. Aleixo · Ana L. C. Lagoa · Manuel E. Minas da Piedade · João P. Leal · Thorsten Peitsch · Matthias Epple

Portuguese Special Chapter
Received: 17 February 2009 / Accepted: 20 March 2009 / Published online: 12 January 2010

Abstract A thermoanalytical, morphological, and structural study of fluoridated calcium phosphates that were prepared by different variants of a synthesis in anhydrous alcohols is reported. The obtained materials were neither fully amorphous nor single-phased crystalline, and their nature considerably depended on the synthesis conditions. In all cases, the retention of significant amounts of solvent in the solid product was observed. A complete removal of the solvent was only possible by heating to temperatures above ~573–673 K which resulted in variations in the elemental composition, phase changes, and an increase of the crystallinity. Consequently, this synthesis in anhydrous alcohols is not a viable route to obtain materials with a defined crystallinity and stoichiometry.

Keywords Calcium phosphates · Apatites · Thermal analysis · Thermogravimetry · Differential scanning calorimetry

R. G. Simões · A. I. Aleixo · A. L. C. Lagoa · M. E. Minas da Piedade (✉) · J. P. Leal
Departamento de Química e Bioquímica, Faculdade de Ciências, Universidade de Lisboa, 1649-016 Lisboa, Portugal
e-mail: memp@fc.ul.pt

J. P. Leal
Unidade de Ciências Químicas e Radiofarmacêuticas, Instituto Tecnológico e Nuclear, 2686-953 Sacavém, Portugal

T. Peitsch · M. Epple
Inorganic Chemistry and Center for Nanointegration Duisburg-Essen, University of Duisburg-Essen, Universitätsstrasse 5-7, 45117 Essen, Germany

Introduction

Calcium phosphates are the inorganic component of human hard tissues, e.g. bone and teeth [1–4]. This has fostered many research efforts to develop biomimetic calcium phosphate materials to be used in medical applications, such as the repair of bone fractures, tooth restoration, or the surface coating of metallic implants to improve their biocompatibility [5–8].

The mineral phase of human hard tissues is a non-stoichiometric hydroxyapatite, whose deviation from the stoichiometric formula, $Ca_{10}(PO_4)_6(OH)_2$, and the crystallite size depend on the biological function [1, 2, 5, 9–12]. The bone mineral, for example, amounts to about half of the total mass of the bone and essentially consists of nanocrystals of a carbonated hydroxyapatite (the so-called "biological apatite"), with the approximate formula $Ca_{10-x}(PO_4,CO_3)_{6-x}(HPO_4)_x(OH)_{2-x}$ [1, 2, 5, 9–13]. Dental enamel, on the other hand, has a larger inorganic content than bone (about 97%) and is formed by larger and strongly oriented prismatic crystals of biological apatite [5].

Fluoridated calcium phosphates are also important biominerals. Shark teeth, for instance, contain fluoroapatite $Ca_{10}(PO_4)_6F_2$ [14, 15], and the replacement of OH^- by F^- in the hydroxyapatite phase of human tooth enamel by fluoridated dental products readily occurs to yield a material similar to hydroxyapatite/fluoroapatite mixed crystals, $Ca_{10}(PO_4)_6(F,OH)_2$, formed in vitro [2, 16–21]. This substitution contributes to the prevention of tooth decay because fluoroapatite is less soluble in the acidic solutions produced by oral bacteria than the original hydroxyapatite present in teeth [22]. It has been noted, however, that the main caries-preventing effect of fluoride is related to its ability to promote the remineralization of teeth using

calcium dissolved in saliva, rather than the formation of fluoridated apatitic phases that are more resistant to acidic attacks [23–25].

Synthetic calcium phosphates are conventionally prepared either by high-temperature solid state reactions or by aqueous precipitation methods [2]. Calcination techniques lead to highly crystalline materials with an increased stability towards dissolution due to a high crystallinity and large crystallites. Hence, in spite of their good biocompatibility, they exhibit low biodegradation rates in vivo compared to the nanosized biological apatites [26, 27]. The drawback of aqueous precipitation routes is the difficult control over stoichiometry caused by the phosphate/hydrogenphosphate equilibrium and, in the case of fluoroapatite, the impossibility to obtain a phase-pure material that contains fluoride only and no hydroxide. Such problems are directly related to the precipitation from the medium water which participates in the reaction. A synthesis in anhydrous alcohols using calcium ethanolate, phosphoric acid, and ammonium fluoride was proposed by Layrolle and Lebugle, which, in principle, allows a better adjustment of the stoichiometry [28, 29]. Here, we report a systematic thermoanalytical and structural study of fluoridated calcium phosphates that were prepared using different variations of this synthesis to investigate if it provides a viable route to produce calcium phosphates with a defined composition and crystallinity.

Experimental

Synthesis

All syntheses were performed using modified versions of the method proposed by Layrolle and Lebugle [29]. The syntheses were carried out under an oxygen- and water-free (<5 ppm) nitrogen atmosphere inside a glove-box or using Schlenk techniques. Metallic calcium (Sigma-Aldrich, 99%, granules), phosphoric acid crystals (Sigma-Aldrich, 99.999%), and ammonium fluoride (Panreac, 95%) were used without further purification. Ethanol (Riedel-de-Häen, p.a.) and *iso*-propanol (Merck, 99.8%) were pre-dried with CaH_2, refluxed under nitrogen with iodine-activated magnesium, and finally distilled. Four families of calcium phosphate samples denoted A to D were prepared and characterized.

Synthesis of samples A1, A2, and A3

In total, 3.0202 g (75.4 mmol) of metallic Ca and 150 cm^3 of ethanol were placed in a three-necked 2 dm^3 round bottom flask inside a glovebox. The setup was removed from the glovebox, connected to a nitrogen line and adapted to a reflux condenser. The mixture was refluxed under nitrogen at 353 K until all the calcium had reacted to calcium ethanolate (~2 h). The solvent was removed in vacuum and $Ca(OEt)_2 \cdot 0.36EtOH$ (9.1 g, 62.0 mmol) was obtained in the form of a fine white powder. Then, 7.0020 g (47.7 mmol) of this sample were dissolved in 200 cm^3 of ethanol inside the glovebox to yield a 0.24 mol dm^{-3} solution of $Ca(OEt)_2$ (S1). A solution of hydrofluoric acid, HF, (S2) was prepared by refluxing 0.4041 g of NH_4F (10.9 mmol) in 200 cm^3 of ethanol inside a 2 dm^3 three necked round bottom flask. The decomposition of NH_4F generates HF according to the reaction [29]:

$$NH_4F\ (sln) \rightarrow\ NH_3\ (g) +\ HF\ (sln) \qquad (1)$$

A 0.215 mol dm^{-3} solution of orthophosphoric acid, H_3PO_4, (S3), produced by dissolving 3.1673 g (32.3 mmol) of solid H_3PO_4 in 150 cm^3 of ethanol inside the glovebox, was transferred to an addition funnel and added dropwise to solution S2 under reflux. Finally, solution S1 was added dropwise to this reaction mixture from a second addition funnel. The formation of a white gelatinous precipitate was immediately observed. The reaction mixture was refluxed under nitrogen atmosphere for 3 h. After cooling, the suspension was transferred to a Schlenk tube and the solvent was removed in vacuum. The obtained solid was dried in vacuum (1.3 Pa), first for 3 days at room temperature and then for another day at 373 K until a constant mass was achieved. The product was divided into three portions: sample A1 was used without further treatment; samples A2 and A3 were heated for 10 h under nitrogen flux at 573 and 873 K, respectively.

Synthesis of samples B1, B2 and B3

The synthesis of these samples was carried out to investigate the effect of excess calcium on the nature of the produced materials. Metallic calcium (3.0983 g, 77.3 mmol) and 200 cm^3 of ethanol were placed into a two-necked round bottom flask inside a glovebox. The reaction system was taken out of the glovebox and connected to a reflux condenser. The mixture was refluxed under nitrogen atmosphere at 353 K until all the calcium had reacted (~10 h) to yield a 0.39 mol dm^{-3} solution of $Ca(EtO)_2$ (S4). A HF solution (S5) was prepared according to reaction (1) by refluxing 0.4138 g of NH_4F (11.2 mmol) in 200 cm^3 of ethanol inside a three-necked 2 dm^3 round bottom flask. A solution of orthophosphoric acid (S6) was prepared by dissolving 3.2546 g (33.2 mmol) of H_3PO_4 in 150 cm^3 of ethanol inside the glovebox. This solution was added to solution S5 under reflux. Finally, solution S4 was added to the reaction mixture with the immediate formation of a white gelatinous precipitate. The resulting suspension was refluxed under nitrogen atmosphere for 1 h. After cooling, the suspension was transferred to a Schlenk tube, the solvent was removed in

vacuum (1.3 Pa), and the obtained solid was dried at room temperature, first for 3 days at 1.3 Pa and subsequently for 7 days at 13 mPa. The product was divided into three portions: sample B1 was used without further processing, and samples B2 and B3 were heated for 17 h under nitrogen flux at 573 and 773 K, respectively.

Synthesis of samples C1, C2 and C3

Metallic calcium (5.0354 g, 125.6 mmol) and 500 cm^3 of ethanol were placed in a three-necked round bottom flask inside a glovebox. The reaction system was removed from the glovebox and connected to a reflux condenser. The mixture was refluxed under nitrogen atmosphere at 353 K until all the calcium had reacted (solution S7). A solution of orthophosphoric acid (S8) was prepared by dissolving 7.5525 g (77.1 mmol) of H_3PO_4 in 300 cm^3 of ethanol inside the glovebox. The vessel containing the solution was taken out of the glovebox and connected to a nitrogen line and to a bubbler containing a concentrated NaOH solution. Gaseous HF was produced in an independent vessel by reacting 5 cm^3 of H_2SO_4 (Panreac, 95%) with 1.0132 g (27.4 mmol) of NH_4F according to

$$H_2SO_4\,(l) + 2NH_4F\,(s) \rightarrow (NH_4)_2SO_4\,(s) + 2HF\,(g) \quad (2)$$

The gas was bubbled into solution S8 to yield solution S9. Solution S7 was then added to solution S9, giving a white precipitate. The resulting suspension was refluxed under nitrogen atmosphere for 2 h, transferred to a Schlenk tube and dried in vacuum at room temperature, first for 3 days at 1.3 Pa and then for 7 days at 13 mPa. The product was divided in three portions: sample C1 was used without further treatment, and samples C2 and C3 were heated for 17 h under nitrogen flux at 573 and 773 K, respectively.

Synthesis of samples D1, D2, D3, and D4

The procedure followed in the preparation of the D samples was essentially the same as described for samples C, except for the use of *iso*-propanol instead of ethanol as solvent. The calcium *iso*-propoxide solution was obtained from 5.0376 g (125.7 mmol) of metallic calcium and 500 cm^3 of *iso*-propanol. An orthophosphoric/hydrofluoric acid mixture was prepared by dissolving 7.5604 g (77.2 mmol) of H_3PO_4 in 300 cm^3 of *iso*-propanol, and bubbling gaseous HF in the obtained solution. The hydrofluoric acid was produced by the reaction of 5 cm^3 of H_2SO_4 (Panreac, 95%) with 1.0197 g (27.5 mmol) of NH_4F. The final reaction mixture was taken to dryness in vacuum at room temperature, and the obtained solid was further dried in vacuum (1.3 Pa) and at 373 K during 4 days. The product was divided into four parts: sample D1 was used without further treatment, and samples D2, D3, and D4 were heated under nitrogen flux for 10 h at 573, 873 and 1173 K, respectively.

Characterization

Elemental analyses (C, H, N) were made with a CE instruments EA-1110 apparatus. The calcium contents of samples A and D were determined with a Pye Unicam SP9 atomic absorption spectrometer (AAS) with an air/acetylene flame. The detection was set to 422 nm and the samples were previously reacted with La_2O_3/HCl. The calcium contents of samples B and C, and the phosphorus contents of all the studied samples were obtained with a Perkin Elmer Optima 2000 DV ion coupled plasma atomic emission spectrometry (ICP) instrument. The fluoride content of all the samples was determined by the potentiometric method reported by Duff and co-workers [30]. A Metrohm 632 pH-Meter, a fluoride selective electrode (Mettler Toledo), and a calomel reference electrode (Metrohm CH-9101 Herisau) were used. Fourier-transform infrared spectra (FTIR) were determined in KBr plates with a Nicolet 6700 instrument. X-ray powder diffractograms (XRD) were recorded on a Philips PW1730 diffractometer (Cu Kα radiation, graphite monochromator). Scanning electron microscopy (SEM) with energy dispersive X-ray spectroscopy (EDX) analyses were performed in high vacuum on Au/Pd-sputtered samples with a FEI ESEM Quanta 400 FEG instrument. Simultaneous thermogravimetric (TG) and differential scanning calorimetry (DSC)

Table 1 Temperatures of the annealing after precipitation, the results of the elemental analysis (mass/%), the molar calcium/phosphorus ratio, *n*(Ca)/*n*(P), and the molar calcium/fluoride ratio, *n*(Ca)/*n*(F), of all samples prepared in this study

Sample	*T*/K	C	H	N	F	Ca	P	*n*(Ca)/*n*(P)	*n*(Ca)/*n*(F)
A/theoretical								1.48	4.38
A1	373	0.36	1.55	1.59	1.02	27.3	21.1	1.00	12.7
A2	573	0.29	0.40	0.42	0.96	26.3	22.7	0.90	13.0
A3	873	0.10	0.02	0.05	0.28	27.7	25.0	0.86	46.9
B/theoretical								2.33	6.90
B1	298	15.33	3.75	0.51	0.03	19.5	6.5	2.32	308.1
B2	573	5.82	0.56	0.21	0.03	18.2	5.8	2.43	287.6
B3	773	1.14	0	0.12	0.04	19.7	6.7	2.27	233.5
C/theoretical								1.69	4.58
C1	298	8.92	1.89	0	0	29.8	17.6	1.31	–
C2	573	1.65	0.97	0	0	32.4	19.5	1.28	–
C3	773	1.04	0.37	0	0	35.1	20.9	1.30	–
D/theoretical								1.63	4.57
D1	373	1.93	1.55	0	0.53	31.3	15.5	1.56	28.0
D2	573	1.83	0.67	0	0.63	29.6	16.3	1.40	22.3
D3	873	0.37	0.09	0	0.70	35.1	18	1.51	23.8
D4	1173	0.18	0	0	0.70	41.4	19.2	1.67	28.0

were performed with a Setaram TG-DSC 111 apparatus. Samples were placed in SiO_2 crucibles and heated from 298 to 873 K at a rate of 3 K min^{-1} under dynamic nitrogen atmosphere (2 dm^3 h^{-1}). Combined thermogravimetric-infrared analysis (TG-IR) and differential thermal analysis (DTA) were carried out on a Netzsch STA 409/Bruker Vertex 70 system (298–1273 K; heating rate 3 K min^{-1}; dynamic nitrogen or oxygen atmosphere, 2 dm^3 h^{-1}; Al_2O_3 crucibles).

Results and discussion

The temperatures used in the final thermal treatment during preparation and the results of the elemental analysis of samples A–D are summarized in Table 1. The results show that the obtained products have a different calcium to phosphorus molar ratio, n(Ca)/n(P), than expected from the amounts of calcium and phosphorus used in the preparations.

The presence of significant amounts of carbon and hydrogen in samples A1, B1, C1, and D1 indicates that the solvent (ethanol or *iso*-propanol) remains partially incorporated in the sample lattice, even after drying in vacuum at a temperature ranging from 298 to 373 K. The carbon and hydrogen contents of the samples decrease with the increase of the annealing temperature, indicating a loss of solvent by evaporation and/or thermal decomposition. The catalytic thermal decomposition of ethanol and *iso*-propanol over calcium phosphates in the range of 523–773 K is well documented, and it is probably the source of the carbon and hydrogen contents of the samples heated above 373 K under nitrogen atmosphere [31]. The nitrogen present in samples A and B originates from residual NH_4^+

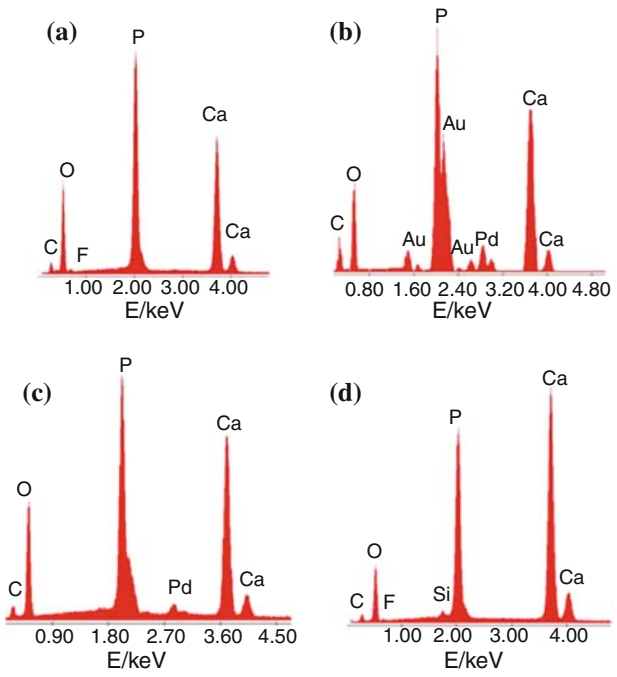

Fig. 1 EDX spectra for samples A1 (**a**), B1 (**b**), C1 (**c**), and D1 (**d**)

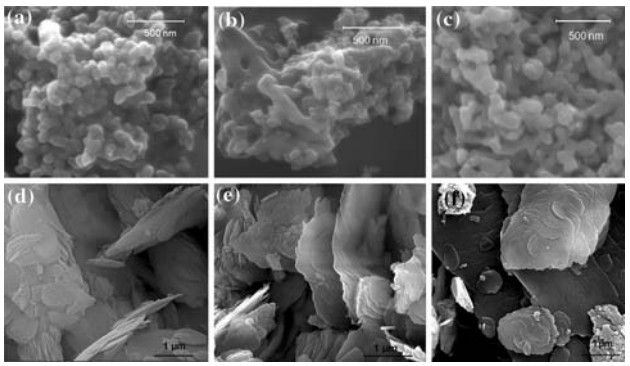

Fig. 2 SEM images of samples **a** A1, heated to 373 K, **b** A2, heated to 573 K, **c** A3, heated to 873 K, **d** C1, heated to 298 K, **e** C2 heated to 573 K, and **f** C3, heated to 773 K

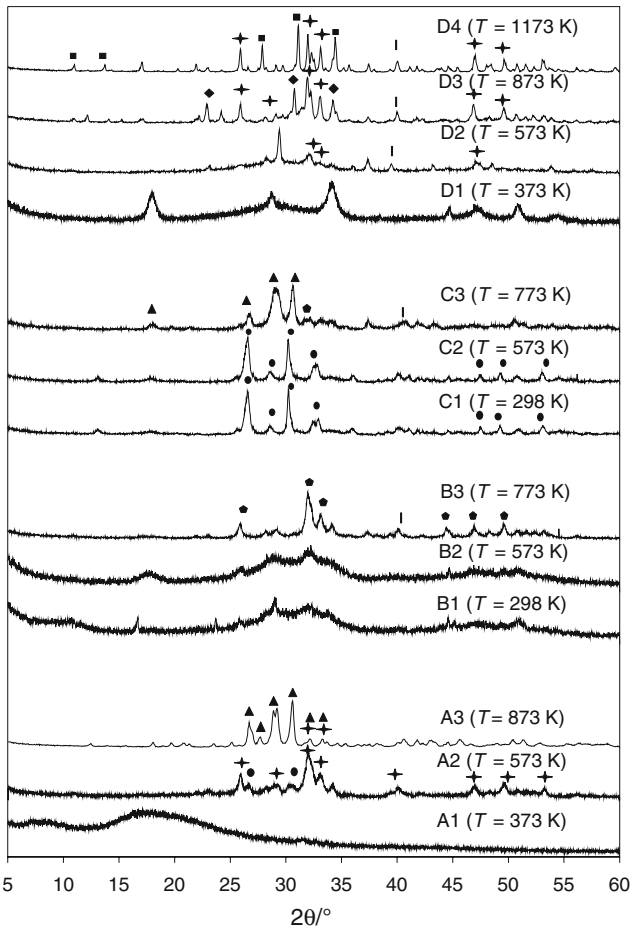

Fig. 3 X-ray powder diffractograms of samples A–D with corresponding preparation temperatures in parenthesis. The marked peaks are assigned to the following phases: hydroxy/fluoroapatite (✦); monetite (•); calcium oxide (|); γ-calcium pyrophosphate (▲); α-calcium pyrophosphate (⬟); α-tricalcium phosphate (◆), and β-tricalcium phosphate (■)

used in the in situ production of HF. This had also been observed by Layrolle and Lebugle in their original synthesis [29]. The nitrogen incorporation in the products was eliminated in the synthesis of samples C and D by the addition of gaseous HF produced externally by reaction (2). The results in Table 1 also indicate that all preparations led to samples with considerably lower fluoride content than those expected from the syntheses. Therefore, the products are highly fluoride-deficient in comparison to stoichiometric fluoroapatite, $Ca_{10}(PO_4)_6F_2$. The fact that the fluoride content also decreased upon heating of the samples A indicates that fluoride was probably not incorporated into the lattice but rather adsorbed on the surface. The samples B showed a n(Ca)/n(P) ratio very close to that used in the synthesis but with almost no incorporation of fluoride. In samples C, no fluoride was incorporated at all, which is unexpected because the difference between the preparations of samples C and D only consisted in the change of the alcoholic solvent.

The results of the EDX analysis (Fig. 1) corroborate the general conclusions drawn from the elemental analysis. Samples A1, B1, C1, and D1 show evidence of carbon from solvent retention in the lattice, and no fluoride is detectable in the case of samples B and C. The trace of Si in Fig. 1d probably results from the HF attack to the glass containers used in the synthesis, and the presence of Au and Pd originates from the sputtering of the samples prior to the SEM analysis.

The SEM micrographs of samples A are shown in Fig. 2a–c. The initially obtained A1 product consisted of compact crystallites with a diameter of about 100 nm, which did not significantly change upon heating. Similar morphologies were observed for samples B and D. In contrast, sample C1 showed a plate-like morphology which did not substantially change upon the heat treatment that led to samples C2 and C3 (Fig. 2d–f).

The X-ray powder diffractograms obtained for all samples are shown in Fig. 3. Note that it is not possible to distinguish between hydroxyapatite and fluoroapatite by conventional X-ray powder diffraction due to the very similar diffraction patterns and also due to the fact that they form a complete substitution row. Therefore, we will denote these phases as hydroxy/fluoroapatite in the following. Except for the samples C, a clear increase of the crystallinity of the products is observed with increasing temperature during the thermal treatment. Sample A1 is practically amorphous. All other samples are more or less crystalline, but they all contain more than one phase. The results of the phase identification through peak assignments using the DIFFRACplus EVA 11.0.0.3 program [32] and the FIZ/NIST database [33] are summarized in Table 2. Analysis of Table 2 suggests that upon heating the initially obtained amorphous A1 material to 573 K, a mixture of monetite and fluoroapatite is formed. Further heating to 873 K leads to pyrophosphate formation by the well-known reaction [34]:

$$2CaHPO_4\ (s) \rightarrow Ca_2P_2O_7\ (s) + H_2O\ (g) \qquad (3)$$

A clear signature of fluoroapatite could not, however, be identified in the diffractogram of sample A3. Samples B1 and B2 are almost amorphous with only traces of hydroxyapatite, and sample B3 corresponds to a mixture of

Table 2 Phase composition of samples A–D as derived from X-ray powder diffraction analysis

Sample	Phase assignment
A1	Amorphous
A2	Mixture of monetite ($CaHPO_4$; JCPDS 00-009-0080) and hydroxy/fluoroapatite (JCPDS 00-034-0011)
A3	α- and γ-calcium pyrophosphate ($Ca_2P_2O_7$; JCPDS 00-009-0345 and JCPDS 00-015-0197) and traces of hydroxy/fluoroapatite (JCPDS 00-034-0011)
B1	Almost amorphous; traces of hydroxy/fluoroapatite (JCPDS 00-034-0011)
B2	Almost amorphous; traces of hydroxy/fluoroapatite (JCPDS 00-034-0011)
B3	Hydroxy/fluoroapatite (JCPDS 01-072-1243) and traces of CaO (JCPDS 37-1497)
C1	Monetite ($CaHPO_4$; JCPDS 00-009-0080)
C2	Monetite ($CaHPO_4$; JCPDS 00-009-0080)
C3	γ-Calcium pyrophosphate ($Ca_2P_2O_7$; JCPDS 00-009-0345); traces of CaO (JCPDS 37-1497), and possibly of hydroxy/fluoroapatite (JCPDS 01-072-1243)
D1	Unknown phase
D2	Mixture of hydroxy/fluoroapatite (JCPDS 00-034-0011), CaO (JCPDS 37-1497), and an unidentified phase
D3	Mixture of hydroxy/fluoroapatite (JCPDS 00-034-0011), α-tricalcium phosphate (α-TCP; α-$Ca_3(PO_4)_2$; JCPDS 00-029-0359), and CaO (JCPDS 37-1497)
D4	Mixture of hydroxy/fluoroapatite (JCPDS 00-034-0011), β-tricalcium phosphate (β-TCP; β-$Ca_3(PO_4)_2$, JCPDS 01-070-2065), and traces of CaO (JCPDS 37-1497)

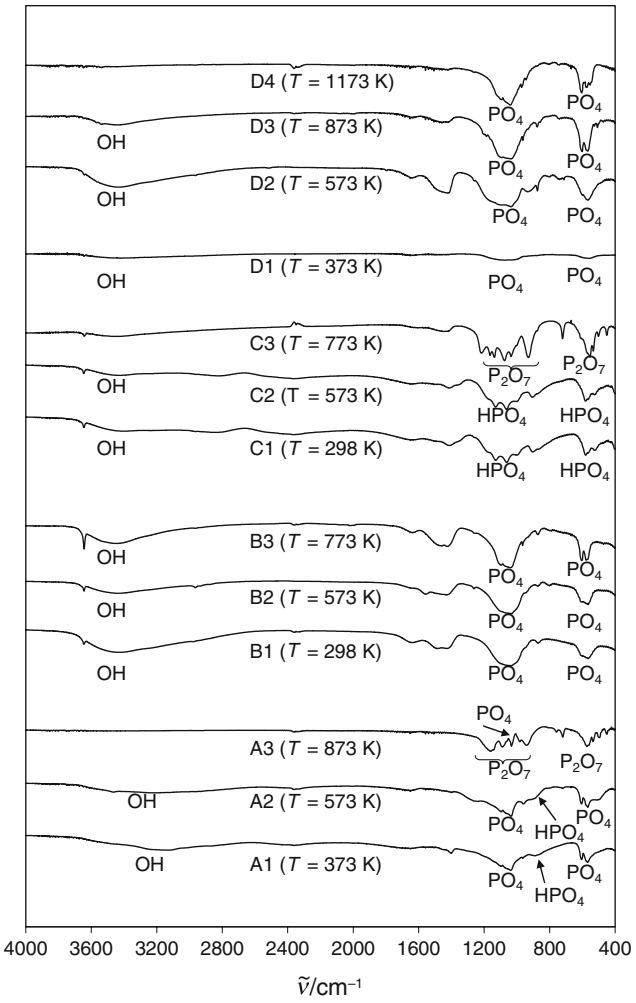

Fig. 4 FTIR spectra of the samples A–D

hydroxyapatite and possibly CaO as indicated by the peak at $2\theta = 37.4°$. Calcium oxide could result from the thermal decomposition of excess $Ca(OEt)_2$ used in the synthesis [35]. The hydroxylation source necessary for the formation of hydroxyapatite may originate from the thermal decomposition of $Ca(OEt)_2$ and ethanol [31, 35]. Note finally that in this case the elemental analysis indicates practically no fluoride in the samples, thus implying the absence of a fluoroapatite phase. Sample C1 corresponds to monetite. Hence, the patterns obtained by successively heating C1 to 573 and 773 K are dominated by the formation of pyrophosphates according to reaction (3) as in the case of samples A and to the thermal decomposition of $Ca(OEt)_2$ leading to CaO. The sample D1 prepared in *iso*-propanol is compatible with a nanocrystalline material, as indicated by the broad peaks observed in the diffraction pattern. The corresponding phase could not, however, be identified. Subsequent heating from 373 to 1173 K leads to a mixture of hydroxy/fluoroapatite, calcium oxide, and β-tricalcium phosphate, $Ca_3(PO_4)_2$.

The FTIR spectra of samples A–D are shown in Fig. 4. The presence of surface-bound and occluded solvent (ethanol or *iso*-propanol) in the samples A1, B1, C1, and D1 is confirmed by the observation of the broad bands in the range 3700–2600 cm^{-1} and at $\sim$1650 cm^{-1}, assigned to O–H stretching and O–H bending modes, respectively [36–38]. Note that water cannot be present due to the fully water-free syntheses. In the case of samples A and D, the observed decrease of the intensity of those bands on heating is consistent with the removal of the solvent and the formation of phases that do not contain hydroxide groups. This is in agreement with the results of X-ray

Table 3 Results of the TG-DSC and TG-IR experiments carried out on samples A1, B1, C1, and D1 in the temperature ranges 298–873 K and 298–1273 K

Method	Sample							
	A1		B1		C1		D1	
	T/K	Δm/%	*T*/K	Δm/%	*T*/K	Δm/%	*T*/K	Δm/%
TG-DSC (N_2)	298–873	10.2	298–657	12.9	298–549	4.7	298–660	7.3
			657–707	3.1	549–751	7.7	660–709	4.7
							709–873	1.1
TG-IR (N_2)	298–902	10.1	298–626	9.8	298–578	1.7	298–655	8.7
	902–910	0.5	626–818	8.1	578–761	8.2	660–707	5.0
			818–1273	6.5	815–947	2.5	707–1173	2.5
TG-IR (O_2)	298–902	10.7					298–660	8.1
	902–910	0.6					660–707	3.8
							840–947	0.6

Note: The mass losses are given as mass percentage (%Δm) and the nature of the purging gas is indicated in parentheses

$\Delta m/\% = 100 \times (m_0 - m)/m_0$ where m_0 is the initial mass of sample and m is the mass of sample at the given temperature in the TG scan

diffraction (Table 2). In contrast, heating samples B1 and C1 to 573 and 773 K did not lead to the elimination of the OH bands. The sharp OH bands at $\sim$3600 cm^{-1} belong to hydroxide groups in hydroxyapatite. The spectra of samples A1 and A2 show the PO_4^{3-} ($\tilde{\nu}$ = 1102, 1043, 607, and 570 cm^{-1}) and HPO_4^{2-} ($\tilde{\nu}$ = 904 cm^{-1}) bands expected for the apatite and monetite phases detected by X-ray diffraction. The disappearance of the HPO_4^{2-} peak at $\tilde{\nu}$ = 904 cm^{-1} and the occurrence of peaks characteristic for $P_2O_7^{4-}$ ($\tilde{\nu}$ = 1160, 985, 720, 550, and 499 cm^{-1}) in sample A3 are also consistent with the X-ray diffraction analysis. The observation of PO_4^{3-} peaks at $\tilde{\nu}$ = 1102, 607, and 570 cm^{-1} in the FTIR spectrum of sample A3 suggests the presence of fluoroapatite, a conclusion that could not be drawn from the X-ray diffraction data. It is, however, unlikely that the fluoroapatite present in sample A2 would decompose upon heating to 873 K. In the case of the samples B, the absence of HPO_4^{2-} bands at $\tilde{\nu}$ = 900 and 1400 cm^{-1} and the presence of PO_4^{3-} peaks (Fig. 4) are also consistent with the X-ray diffraction results. These indicate the formation of a hydroxyapatite phase upon heating from 298 to 773 K and show no evidence of hydrogenphosphate-containing phases (e.g. monetite) or pyrophosphate originating from their decomposition through reaction (3). The FTIR spectra of the samples C1 and C2 show the HPO_4^{2-} peaks (Fig. 4) expected for the monetite phase indicated by the X-ray diffraction analysis. The decomposition of this phase on heating according to reaction (3) is also evidenced by the presence of peaks attributed to $P_2O_7^{4-}$ in the FTIR spectrum of sample C3. The FTIR spectra of samples D show the presence of PO_4^{3-} peaks (Fig. 4) consistent with the presence of fluoroapatite and tricalcium phosphate phases observed by X-ray diffraction.

Table 3 summarizes the TG-DSC (298–873 K) and TG-IR (298–1273 K) results obtained for samples A1, B1, C1, and D1. Figure 5 shows an overlay of three measuring curves corresponding to sample A1: TG in the range of 298–1273 K, DSC in the range of 298–873 K, and DTA in the range of 873–923 K. The DTA experiment was run to complement the DSC results which (due to instrumental limitations) were only performed up to 873 K. It should also be noted that the relative intensities of the DSC and DTA peaks in Fig. 5 are not comparable in absolute terms, as they were scaled relative to their minimum values in the temperature ranges covered by the experiments.

Figure 5 also shows several IR spectra of the gases evolved during the thermogravimetric experiment. A mass loss of about 10% up to 873 K with two or three unresolvable steps is observed. The accompanying decrease in heat flow observed in the DSC measurements where at least three small unresolved peaks are evident indicates that it corresponds to a complex endothermic process. The

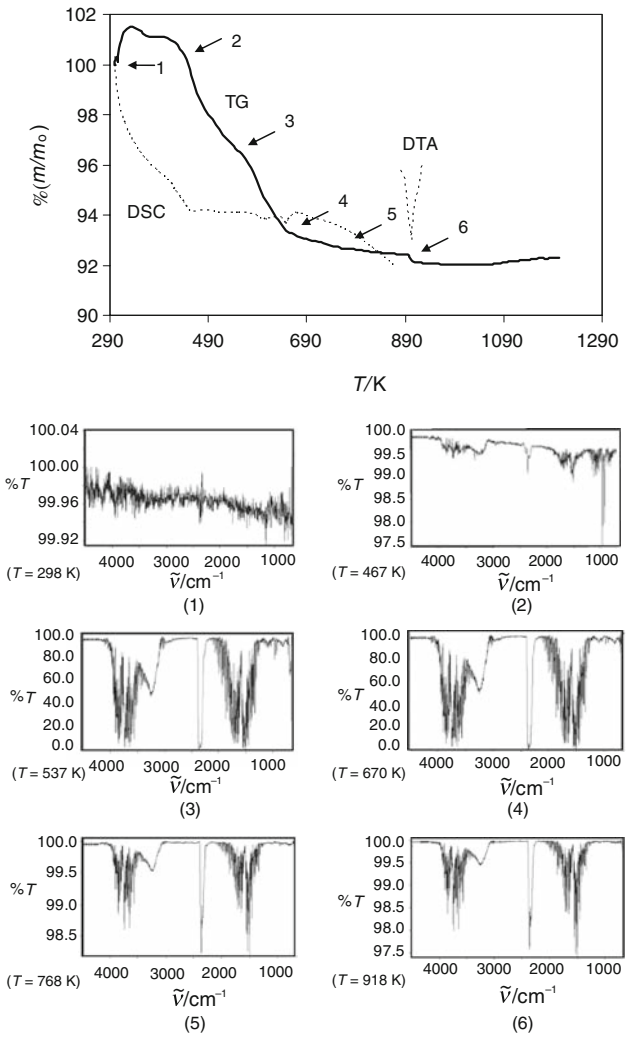

Fig. 5 Results of TG-IR, DSC and DTA experiments on sample A1, using nitrogen as the purging gas. The scale on the left corresponds to the sample mass percentage 100 × (m/m_0) determined in the TG experiments. The numbered IR spectra refer to the given temperatures. In the DSC and DTA measuring curves, peaks corresponding to endothermic events point downwards

observation of a band at $\tilde{\nu} \sim 1000$ cm^{-1} in the IR spectrum 2 at 467 K suggests ethanol evaporation up to $\sim$473 K. This is followed by its thermal decomposition as shown by the formation of H_2O and CO_2 between $\sim$533 K and $\sim$673 K (IR spectra 3 and 4 in Fig. 5). The thermal decomposition of HPO_4^{2-} accompanied by the release of water according to reaction (3) may also contribute to the mass loss observed in this range. This reaction was indeed reported to be endothermic and occur in a wide range ($\sim$573–973 K) without a resolvable mass loss step [34, 39]. Finally, the nature of the small mass loss (0.5–0.6%) at $\sim$903 K with H_2O and CO_2 release, also detected by DTA, could not be determined.

As shown by the overlay of the TG data for samples A1–D1 in Fig. 6, the initial and pronounced mass loss due

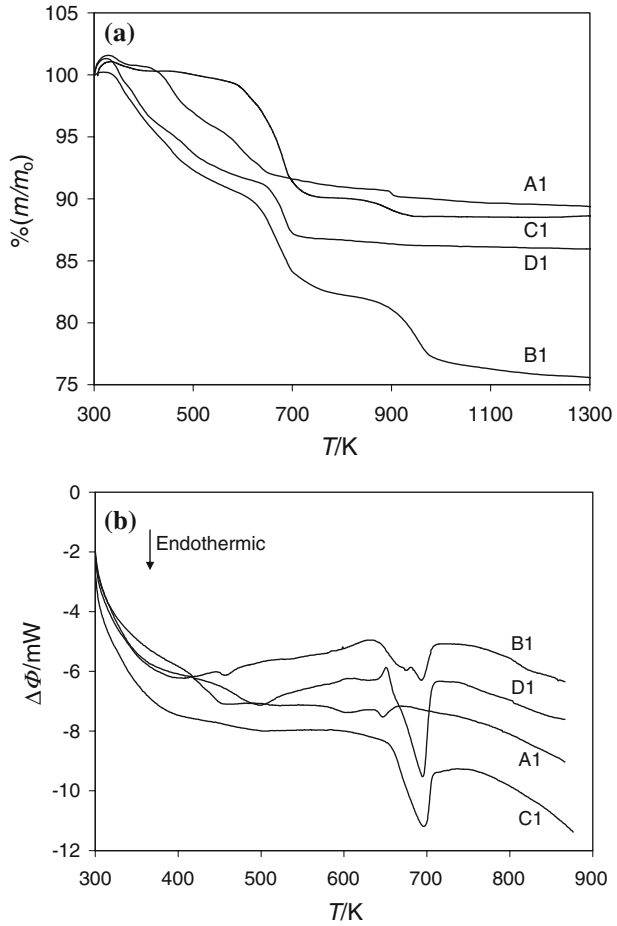

Fig. 6 Overlays of the TG curves (**a**) and the DSC curves (**b**) obtained for the samples A1–D1

to solvent evaporation/thermal decomposition and eventually reaction (3) detected for sample A1 was also observed for samples B1, C1, and D1. Note that all samples show a clear endothermic DSC peak at ~673 K. This peak is within the range typical of the thermal decomposition of HPO_4^{2-} in accordance with reaction (3) [34, 39] (see above). It cannot, however, be unequivocally assigned to this process because the presence of hydrogenphosphate or pyrophosphate is evident by X-ray diffraction (Fig. 3) and FT-IR analysis (Fig. 4) of samples A and C, but it is not clear in the corresponding results for samples B and D.

Conclusions

The nature of fluoridated calcium phosphates obtained by water-free precipitation from alcoholic media studied in this work is very sensitive to variations of the synthetic conditions. The fluoridation of the products by in situ NH_4F decomposition during synthesis seems to be more efficient than the use of an HF solution, but it leads to the incorporation of NH_4^+ in the structure. The retention of significant amounts of solvent in the solid product even after drying in vacuum at temperatures between ~298 and 373 K is a severe drawback of this type of synthesis to produce materials with a defined composition and crystallinity. A more complete removal of the solvent is achieved by heating the materials to temperatures above ~573 K but this leads to a significant increase of crystallinity and to structural changes due to decomposition reactions involving, e.g. hydrogenphosphate.

Acknowledgements This work was supported by Fundação para a Ciência e a Tecnologia (FCT, Portugal) and the CRUP (Portugal; A-31/09)/DAAD (Germany) bilateral exchange program. PhD and Post Doctoral grants from FCT are also gratefully acknowledged by R.G.S. (SFRH/BD/48410/2008) and A.L.C.L. (SFRH/BPD/35053/2007), respectively.

References

1. LeGeros RZ. Biological and synthetic apatites. In: Brown PW, Constantz B, editors. Hydroxyapatite and related materials. Boca Raton: CRC Press; 1994.
2. Elliot JC. Structure and chemistry of the apatites and other calcium orthophosphates. Amsterdam: Elsevier; 1994. p. 208.
3. Baeuerlein E. Biomineralization. Progress in biology, molecular biology and application. Weinheim: Wiley-VCH; 2004.
4. Epple M, Baeuerlein E. Biomineralisation: medical and clinical aspects. Weinheim: Wiley-VCH; 2007.
5. Dorozhkin SV, Epple M. Biological and medical significance of calcium phosphates. Angew Chem Int Ed. 2002;41:3130–46.
6. Salinas AJ, Vallet-Regi M. Evolution of ceramics with medical applications. Z Anorg Allg Chem. 2007;633:1762–73.
7. Vallet-Regi M, Gonzalez-Calbet JM. Calcium phosphates as substitution of bone tissues. Prog Solid State Chem. 2004;32:1–31.
8. Kenny SM, Buggy M. Bone cements and fillers: a review. J Mater Sci Mater Med. 2003;14:923–38.
9. Weiner S, Wagner HD. The material bone: structure-mechanical function relations. Annu Rev Mater Sci. 1998;28:271–98.
10. Wopenka B, Pasteris JD. A mineralogical perspective on the apatite in bone. Mater Sci Eng C. 2005;25:131–43.
11. Rey C, Combes C, Drouet C, Sfihi H, Barroug A. Physico-chemical properties of nanocrystalline apatites: implications for biominerals and biomaterials. Mater Sci Eng C. 2007;27:198–205.
12. Horvath AL. Solubility of structurally complicated materials: II. bone. J Phys Chem Ref Data. 2006;35:1653–69.
13. Peters F, Schwarz K, Epple M. The structure of bone studied with synchrotron X-ray diffraction, X-ray absorption spectroscopy and thermal analysis. Thermochim Acta. 2000;361:131–8.
14. Moller IJ, Melsen B, Jensen SJ, Kirkegaard E. A histological, chemical and X-ray diffraction study on contemporary (*Carcharias glaucus*) and fossilized (*Macrota odontaspis*) shark teeth. Arch Oral Biol. 1975;20:797–802.
15. Daclusi G, Kerebel LM. Ultrastructural study and comparative analysis of fluoride content of enameloid in sea-water and freshwater sharks. Arch Oral Biol. 1980;25:145–51.
16. Jha LJ, Best SM, Knowles JC, Rehman I, Santos JD, Bonfield W. Preparation and characterization of fluoride-substituted apatites. J Mater Sci Mater Med. 1997;8:185–91.
17. Manjubala I, Sivakumar M, Nikkath SN. Synthesis and characterisation of hydroxy/fluoroapatite solid solution. J Mater Sci. 2001;36:5481–6.

18. Rodriguez-Lorenzo LM, Hart JN, Gross KA. Influence of fluorine in the synthesis of apatites. Synthesis of solid solutions of hydroxy-fluorapatite. Biomaterials. 2003;24:3777–85.
19. Gross KA, Rodriguez-Lorenzo LM. Sintered hydroxyfluorapatites. Part I: sintering ability of precipitated solid solution powders. Biomaterials. 2004;25:1375–84.
20. Busch S, Schwarz U, Kniep R. Morphogenesis and structure of human teeth in relation to biomimetically grown fluorapatite–gelatine composites. Chem Mater. 2001;13:3260–71.
21. Prymak O, Sokolova V, Peitsch T, Epple M. The crystallization of fluoroapatite dumbbells from supersaturated aqueous solution. Cryst Growth Des. 2006;6:498–506.
22. Bartlett JD, Dwyer SE, Beniash E, Skobe Z, Payne-Ferreira TL. Fluorosis: a new model and new insights. J Dent Res. 2005;84:832–6.
23. ten Cate JM, Duijsters PPE. Influence of Fluoride in solution on tooth demineralization. 2. Microradiographic data. Chemical-data. Caries Res. 1983;17:513.
24. Cate JM, Duijsters PPE. Influence of Fluoride in solution on tooth demineralization. 1. Chemical-data. Caries Res. 1983;17:193–9.
25. Ögaard B, Rolla G, Ruben J, Dijkman T, Arends J. Microradiographic study of demineralization of shark enamel in human caries model. Scand J Dent Res. 1988;96:209–11.
26. Tadic D, Peters F, Epple M. Continuous synthesis of amorphous carbonated apatites. Biomaterials. 2002;23:2553–9.
27. Tadic D, Epple M. A thorough physicochemical characterisation of 14 calcium phosphate-based bone substitution materials in comparison to natural bone. Biomaterials. 2004;25:987–94.
28. Layrolle P, Lebugle A. Characterization and reactivity of nanosized calcium phosphates prepared in anhydrous ethanol. Chem Mater. 1994;6:1996–2004.
29. Layrolle P, Lebugle A. Synthesis in pure ethanol and characterization of nanosized calcium phosphate fluoroapatite. Chem Mater. 1996;8:134–44.
30. Duff EJ, Stuart JL. Determination of fluoride in calcium phosphates with a fluoride-selective electrode. Anal Chim Acta. 1970;52:155–7.
31. Monma H. Catalytic behavior of calcium phosphates for decompositions of 2-propanol and ethanol. J Catal. 1982;75:200–3.
32. DIFFRACplus EVA 11.0.0.3. Karlsruhe: Bruker AXS; 1996–2005.
33. FIZ/NIST Inorganic Crystal Structure Database (ICSD), NIST Standard Reference Database 84. Gaithersburg: National Institute of Standards and Technology; 2006.
34. Wikholm NW, Beebe RA, Kittelberger JS. Kinetics of the conversion of monetite to calcium pyrophosphate. J Phys Chem. 1975;79:853–6.
35. Dongare MK, Sinha APB. Thermal analysis of some metal alkoxides. Thermochim Acta. 1982;57:37–45.
36. Klee WE, Engel G. I.R. spectra of the phosphate ions in various apatites. J Inorg Nucl Chem. 1970;32:1837–43.
37. Fowler BO. Infrared studies of apatites. I. Vibrational assignments for calcium, strontium, and barium hydroxyapatites utilizing isotopic substitution. Inorg Chem. 1974;13:194–207.
38. Penel G, Leroy G, Rey C, Sombret B, Huvenne JP, Bres E. Infrared and Raman microspectrometry study of fluor-fluor-hydroxy and hydroxy-apatite powders. J Mater Sci Mater Med. 1997;8:271–6.
39. Berry EE. The structure and composition of some calcium-deficient apatites. J Inorg Nucl Chem. 1967;29:317–27.